Research Article

Angi Chen*, Yan Zhao*, Hongda Chen, Huachao Ma, and Kuilin Lv*

Facile design of PTFE-kaolin-based ternary nanocomposite as a hydrophobic and high corrosion-barrier coating

https://doi.org/10.1515/rams-2024-0019 received January 23, 2024; accepted April 10, 2024

Abstract: Superhydrophobic nanostructured coatings are a promising technology in construction engineering. This study developed a hydrophobic film through a simple mixing method, utilizing kaolin and polytetrafluoroethylene as additive particles, 1H,1H,2H,2H-perfluoro-decyl triethoxysilane as a modifier, and epoxide resin and polyamide curing agent as adhesives. By controlling variables, it was determined that the C₁P_{0.2}EP coating immersed in a 3.5 wt% NaCl solution for 1, 3, and 7 days exhibited the maximum impedance radii of 47,373, 20,334, and 1,982 Ω·cm², respectively. It also demonstrated the highest Bode modulus values, the largest E_{corr} , and the smallest I_{corr} . Furthermore, after 300 h in a salt spray chamber with a 3.5 wt% NaCl solution, the C₁P_{0.2}EP coating showed no rust spots or bubbles, demonstrating its excellent corrosion resistance. Moreover, wear resistance tests and selfcleaning experiments were conducted on the C₁P_{0.2}EP coating. The results showed that after 100 friction cycles, the surface exhibited no visible scratches, and the contact angle of the coating decreased by only 4°. Additionally, neither soil particles nor dirty water adhered to the coating, indicating that the C₁P_{0.2}EP hydrophobic coating possesses not only excellent corrosion resistance but also superior wear resistance and self-cleaning capabilities.

Huachao Ma: State Key Laboratory of Green Building Materials, China State Building Materials Research Institute Co, Ltd. Room, Chaoyang District, Beijing, China

Keywords: metal corrosion, PTFE, hydrophobic, anticorrosive coatings

1 Introduction

At present, hydrophobic coatings have a broad application prospect in civil, architectural, and even national defense fields. With the rapid development of science and technology, methods, such as etching, electrostatic spinning, template, vapor deposition, gel film injection, and phase separation, have been increasingly applied to prepare hydrophobic coatings [1–4]. These technologies expand the choice of researchers in material preparation and significantly reduce the threshold and cost of applying hydrophobic coatings [5,6]. Therefore, the basic test and theoretical research of hydrophobic coatings are relatively mature, and the synthesis methods are also rich and diverse. However, the practical application of hydrophobic coatings still needs several significant problems.

First of all, many preparation methods of hydrophobic coatings are only suitable for laboratory development, or the preparation cost is high, which makes it challenging to solve large-scale industrial applications. Therefore, it is urgent to find a preparation method suitable for large-scale industrial applications. For example, Nakajima et al. [7] added sublimable Al(C5H7O2)3 to silica sol and coated the oxide coating on the surface of Q235 steel. The surface of the coating is hydrophobic after fluorination of perfluoroalkyl chlorosilane. However, the sublimation temperature of Al(C₅H₇O₂)₃ is as high as 193°C, which significantly limits large-scale industrial production. Moreover, some processes of preparing hydrophobic coatings also use a lot of organic solvents, which will cause irreversible harm to the environment. Some preparation methods have higher requirements on the substrate, and maybe this method is only suitable for a specific substrate, such as glass or metal surface [8-10].

Although the improvement of preparation technology has brought much convenience to superhydrophobic

^{*} Corresponding author: Anqi Chen, School of Civil Engineering and Architecture, Wuyi University, Fujian Province, China,

e-mail: caqqczj@wuyiu.edu.cn

^{*} Corresponding author: Yan Zhao, School of Civil Engineering and Architecture, Wuyi University, Fujian Province, China,

e-mail: zhaoyan_hit@163.com

^{*} Corresponding author: Kuilin Lv, State Key Laboratory of Green Building Materials, China State Building Materials Research Institute Co, Ltd. Room, Chaoyang District, Beijing, China, e-mail: lv_k_l@163.com Hongda Chen: Nanping Management Branch, Fujian Province High Speed Group Co., Ltd, Fujian Province, China

coatings, most of the coatings prepared at the existing technical level still need better service life, which will also restrict their development in practical application [11-14]. Generally, the surface of the hydrophobic coating is easily damaged or peeled off in some situations, such as impact, friction, and even touch, and most of the damage is irreversible. Nowadays, many researchers are committed to improving the wear resistance of hydrophobic coatings, including self-healing and surface self-repair. Currently, it is challenging for hydrophobic materials to possess both superhydrophobic properties and excellent corrosion resistance, abrasion resistance, and self-cleaning capabilities simultaneously [15]. Jena et al. used a simple method of electrodeposition to prepare a nickel (Ni) reduced graphene oxide (rGO)-myristic acid superhydrophobic (SHP) coating on carbon steel (CS), resulting in a superhydrophobic coating with superior corrosion resistance and self-cleaning abilities [16]. Zhu et al. [17] prepared a hydrophobic metal/polymer composite coating that is easy to self-repair. After mechanical wear, the surface can maintain a rough texture and superhydrophobicity. However, when the hydrophobic angle decreases after wear, the hydrophobicity can be restored by simple fluorination. Cao et al. [18] developed a silicon-based superhydrophobic coating with high adhesion, wear resistance, and damage healing. Tests show that when the surface of the coating is mechanically worn and loses its hydrophobicity, its hydrophobicity can be restored by simple heat treatment because the dynamic molecules of supramolecular polymer in the coating will cross-link. In addition, the stability and durability of the hydrophobic coatings usually prepared could be better, which will seriously affect the service life and application scope of hydrophobic coatings. Therefore, only when the coating process is suitable for large-scale preparation and the obtained hydrophobic coating has good stability and durability can it have practical value for civil and commercial use.

According to the corrosion mechanism, metal corrosion can be divided into electrochemical corrosion, chemical corrosion, and physical corrosion. Among these corrosions, electrochemical corrosion is the most common. Corrosion of metals by atmosphere, seawater, soil, and various electrolytes belongs to electrochemical corrosion. In industrial production, many metal materials will be affected by oxygen in the air and produce electrochemical corrosion. Therefore, if a hydrophobic coating is coated on the metal surface to isolate it from water and air, it can achieve anticorrosion. Because of its hydrophobicity, it can play a role in anticorrosion and weather resistance for a long time. Polyurethane resin and epoxy resin first appeared in the 1950s. Their appearance

significantly improved the corrosion resistance of coatings. In composite coatings, the well-distributed modified graphene oxide (GO) inside the polymer matrix provides extra torturous paths for the permeation of corrosive mediums [19]. Chang et al. [20] successfully prepared super hydrophobic graphene/epoxy resin coatings. Functionalized graphene prepared by thermal reduction can be uniformly dispersed in an epoxy resin coating solution, and adding a small amount of graphene can play an excellent physical barrier role and significantly improve the corrosion resistance of the coating. Liu et al. [21] added a small amount of graphene to waterborne epoxy coatings, and the Tafel polarization curve tested the corrosion resistance of graphene-based epoxy coatings. Generally speaking, the development trend of anticorrosion coatings is strong corrosion resistance, environmental friendliness, and reduced production costs [22].

Polytetrafluoroethylene (PTFE) is known as the 'king of plastics' because of its excellent resistance to both acid and alkali medium, so the coatings composed of PTFE have an attractive application prospect in the field of corrosion protection [23]. Even though commercially coating systems, such as epoxy resin, have been used as structural coatings, the challenges are the defeats or voids experienced in these coatings during curing stages that hinder their long-term barriers' performance. Also, low damage tolerance often leads to premature coating degradation [24,25]. A superhydrophobic PTFE coating on the stainless-steel surface with a high stability and versatile performance was fabricated by the simple electrodeposition and high-temperature curing [26]. Corrosion behavior of enamel-coated reinforcing steel bars in 3.5 wt% NaCl solution is evaluated by open-circuit potential, electrochemical impedance spectroscopy (EIS), and potentiodynamic polarization testing.

In this study, we selected kaolin and polytetrafluoroethylene (PTFE) as additive particles to provide corrosion resistance to the film. 1H,1H,2H,2H-perfluoro-decyl triethoxysilane (PFDTES) was chosen as a modifier to modify kaolin and PTFE, forming a three-dimensional stacked structure that confers excellent wettability to the film. Epoxide resin (EP) and polyamide curing agent (PA) were used as adhesives to enhance the film's superior abrasion resistance and self-cleaning ability, thereby creating a wear-resistant hydrophobic film. Herein, after much experimental research, the optimum addition of modifier is 0.2 ml, and kaolin is 1 g. This is because the filler determines the comprehensive properties of the composite. The combination of modified kaolin filler and epoxy resin can provide mechanical solid strength and hardness and provide a rich micro-nano-scale layered rough structure to improve the hydrophobic performance of the composite. These results suggest that doping the optimized

content of kaolin could form a nano-network covering the micropores to impede the diffusion of corrosive medium.

970F) was used to evaluate the thickness of the coatings, and we measured three times to take the average value. Static contact angle measurements were performed via contact angle meter (KSV instruments, Finland) using a sessile drop technique.

2 Experimental

2.1 Materials

Nano kaolin (99.99%), PTFE (99.9%), and PFDTES (96%) were purchased from Alfa Aesar. EP, PA, defoamer, and cosolvent were purchased from Guangzhou Zhongwan New Material Co., Ltd. Q235 steel (ingredient: $C \le 0.22\%$, Mn \leq 1.4%, Si \leq 0.35%, S \leq 0.050%, P \leq 0.045; size: 0.2 mm \times 30 mm × 30 mm), and ethanol was obtained from Modern Oriental Technology Development Co., Ltd.

2.2 Preparation of epoxy hydrophobic coatings

The steel plate was polished with 180-mesh sandpaper to remove any oil and rust. The steel plate was ultrasonically washed with distilled water and anhydrous ethanol for 10 min each, followed by drying in an oven.

In 3.3 ml of anhydrous ethanol, 0.5 g, 1 g, 1.2 g, 1 g and 1.5 g of kaolin nanopowder, 0.33 g of EP and 0.33 g of PTFE powder were added and dispersed by ultrasuonication for 20 min with magnetic stirring for 2 h at room temperature to obtain the final mixed emulsion. Then, 0.1, 0.15, 0.2, and 0.3 ml of modifier PFDTES were added to the mixed emulsion with stirring, and the mixture was stirred at room temperature for 2h; 0.33 g of PA was added into the emulsion mixed solution, and the mixture was continuously stirred at room temperature for 30 min to obtain a pre-cured mixed emulsion; The pre-cured mixed emulsion was dripped on Q235 steel electrode sheet and glass sheet substrate and finally dried and cured for 24 h at room temperature. The resulting coating is designated as $C_x P_v EP$ (x and y represent the respective contents of kaolin and PFDTES, respectively) coatings.

2.3 Characterizations

The surface morphologies of samples were observed under a Field Emission Scanning Electron Microscope (FESEM) (JEOL, JSM-7500F, Japan). An optical microscope (KEYENCE, VHX-

2.4 Electrochemical measurements

Electrochemical experiments were performed on the electrochemical workstation (Zahner-Electrik IM6e), and 3.5 wt% NaCl solution was used as the electrolyte. The three electrodes system was adopted, in which the working electrode, Ag/AgCl electrode (the saturated KCl solution), and Pt sheet were used as the counter electrodes, respectively. The effective surface area of the working electrode for EIS was measured to be 1 cm², with a step size of 2 s for the corrosion potential measurement. The test employed an amplitude of 10 mV and a frequency range spanning from 10 mHz to 10 kHz. Prior to the measurements, the coating was immersed in a 3.5 wt% NaCl solution until a stable open-circuit potential was achieved. Tafel potential polarization tests were then conducted at a constant current rate of $1 \text{ mV} \cdot \text{s}^{-1}$ to determine the corrosion potential (E_{corr}) and corrosion current density (I_{corr}) through Tafel extrapolation. To ensure the scientificity and repeatability of the electrochemical data, parallel experiments were performed and repeated five times.

2.5 Wear resistance test and self-cleaning experiment

In the abrasive paper test, the hydrophobic film-coated glass substrate was brought into contact with 1,000-grit abrasive paper. Both the abrasive paper and the substrate were loaded with a 500 g weight, and an external force was applied to push them horizontally along a ruler to a distance of 3 cm, constituting one cycle. The change in hydrophobic angle was measured every 10 wear cycles. After 100 cycles, the surface condition of the hydrophobic film and the trend of hydrophobic angle changes were observed. In the self-cleaning experiment, soil particles were sprinkled onto the glass substrate and it was immersed in dirty water. The glass substrate was then tilted and removed from the dirty water. The self-cleaning ability of the hydrophobic film was judged by observing whether any stains adhered to the surface of the film.

4 — Angi Chen et al. DE GRUYTER

3 Results and discussion

3.1 Characterization of samples and coatings

3.1.1 Performance characterization of epoxy hydrophobic coatings

The super wettability of a solid surface is closely related to its microstructure and chemical composition. The SEM test results for the coatings C_{0.5}P_{0.2}EP, C₁P_{0.2}EP, C_{1.2}P_{0.2}EP, and C_{1.5}P_{0.2}EP are presented in Figure 1. Figure 1(a) shows the SEM results for the $C_{0.5}P_{0.2}EP$ coating. It can be observed that the C_{0.5}P_{0.2}EP coating exhibits a scattered particle structure rather than a three-dimensional structure. This is due to the insufficient amount of kaolin added, resulting in kaolin and PTFE particles scattered on the epoxy resin film, insufficient to form a three-dimensional stacked structure. Figure 1(b) displays the SEM results for the C₁P_{0.2}EP coating. As can be seen, when the content of kaolin increases to 1g, kaolin and PTFE form a three-dimensional stacked structure under the action of modifiers. Multiple pores are formed between the layers, which can absorb air and improve the wettability of the coating, thereby increasing the hydrophobic angle of the coating. Figure 1(c) presents the SEM results for the C_{1.2}P_{0.2}EP coating. Since the content of PTFE remains unchanged, when the content of kaolin increases to 1.2 g, excess kaolin particles block the pores between the three-dimensional stacked structures, reducing the coating's ability to trap air and consequently leading to a decrease in the hydrophobic angle. Figure 1(d) demonstrates the SEM results for the C_{1.5}P_{0.2}EP coating. As the content of

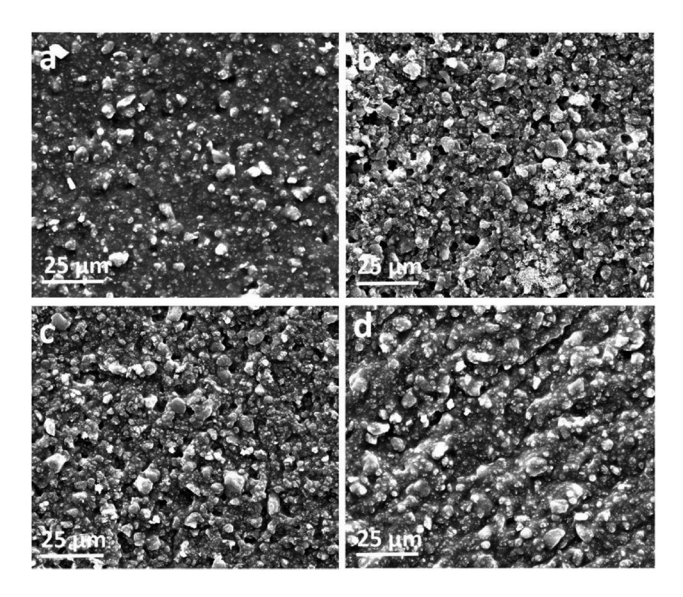


Figure 1: SEM images of $C_{0.5}P_{0.2}EP$ (a), $C_1P_{0.2}EP$ (b), $C_{1.2}P_{0.2}EP$ (c), and $C_{1.5}P_{0.2}EP$ (d).

kaolin further increases, excess kaolin particles continue to block the pores between the three-dimensional stacked structures and form cracks, further reducing the hydrophobic angle of the coating. Based on the SEM results, the $C_1P_{0.2}EP$ coating exhibits the best wettability, characterized by the largest hydrophobic angle.

Using a contact angle measuring instrument, we determined the water contact and sliding angles of superhydrophobic materials on various substrates, documenting the macroscopic hydrophobic properties of different samples through photography. As evident in Figure 2, the conjunction of appropriate roughness and low surface energy materials confers hydrophobic properties to materials fabricated on different substrates. Notably, water droplets maintain a spherical shape on these surfaces, indicating remarkable hydrophobicity.

Figure 2(a) illustrates that within 60 days, the water contact angles of coatings formulated with varying quantities of four modifiers all exceed 136°, signifying low surface energy and robust hydrophobicity. The addition of modifiers creates a more convoluted path for water absorption in the epoxy coating, effectively barricading the infiltration of corrosive ions and reducing the adherence of corrosive media to the coating surface, thereby decelerating substrate corrosion. Over time, the water contact angles of these coatings decrease, with the C_{1.2}P_{0.1}EP coating exhibiting the most notable decline. Nevertheless, the C_{1.2}P_{0.2}EP coating maintains the highest water contact angle, surpassing 142° even after 60 days, reflecting its superior hydrophobicity and low porosity. To further explore the influence of kaolin content on water wettability, we examined the water contact angles of four coatings with varying kaolin concentrations.

Figure 2(b) depicts the evolution of water contact angles for coatings with four different kaolin contents as soaking time increases. During the initial soaking stage, all four coatings with varying kaolin contents exhibited hydrophobic angles exceeding 120°, indicating their robust hydrophobic properties. As depicted in the figure, as kaolin content rises, the hydrophobic angle initially climbs before leveling off, possibly due to the aggregation phenomenon and the swelling of micro-pockets on the coating surface with increasing kaolin content. When kaolin content reaches 0.5 g, the hydrophobic angle is at its lowest, while coatings containing 1 g of kaolin yield the highest hydrophobic angle, exceeding 147°. Over time, the hydrophobic angles of these coatings decline marginally, but the reduction is minor, with less than 5° decrease within 60 days. This suggests that kaolin effectively fills pores on the epoxy resin surface, reducing porosity. Notably, the coating with 1 g of kaolin consistently maintains the highest hydrophobic angle, lowest porosity, and superior hydrophobic performance.

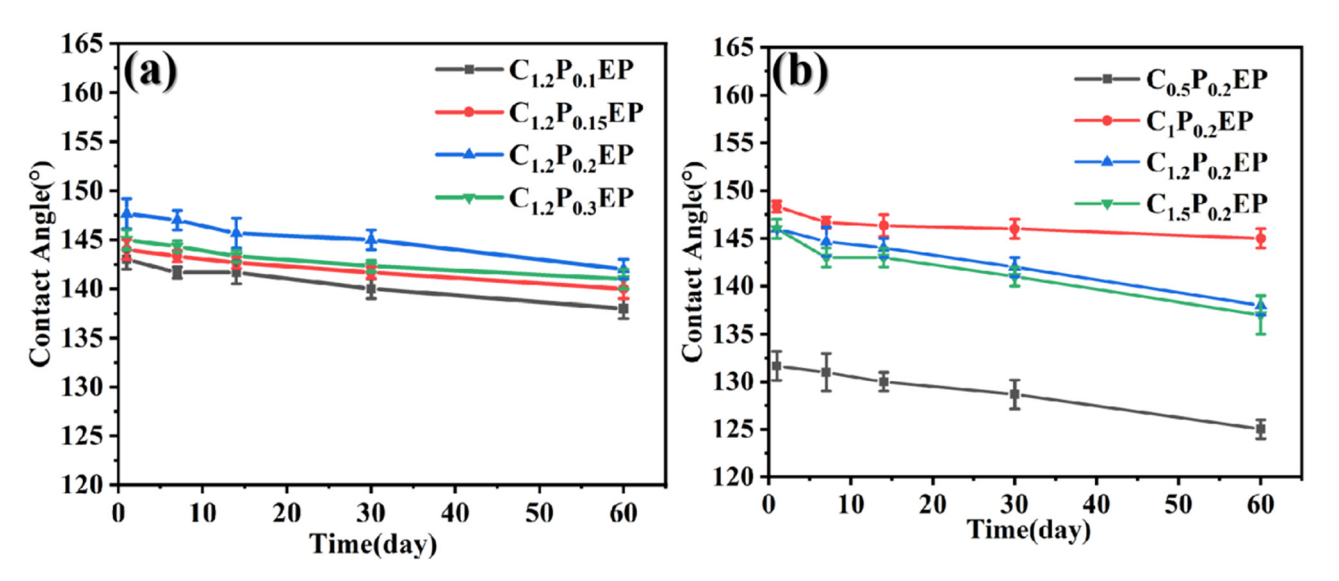


Figure 2: Variation of contact angle values with time at room temperature (a) 1.2P0.1EP,C1.2P0.15EP,C1.2P0.2EP,C1.2P0.3EP, (b) C0.5P0.2EP,C1P0.2EP,C1.2P0.2EP,C1.5P0.2EP.

3.2 Electrochemical properties of GEP coatings

3.2.1 Effect of additive amount on corrosion resistance of coating

The influence of modifier (PFDTES) addition on the corrosion resistance of epoxy resin coating was investigated by

the control variable method. Figure 3 shows the EIS and Bode of coatings with different modifier concentrations immersed in 3.5 wt% NaCl solution for various durations, and the specific data are presented in Table 1. In general, the larger the diameter of the semicircle in the Energy Quest diagram, the greater the impedance and the better the corrosion resistance of the coating. As shown in Figure 3(a), on the first day of soaking, the Nyquist diagram

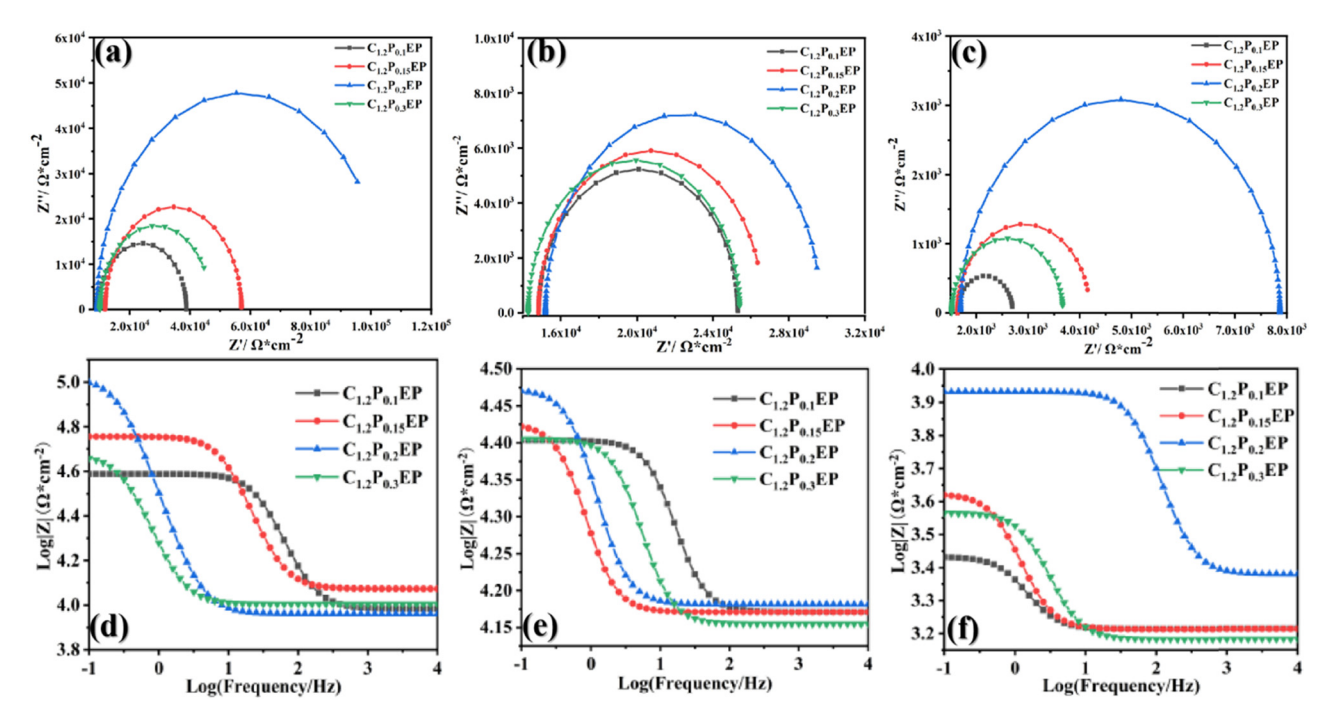


Figure 3: EIS and Bode plots of coatings with different modifier concentrations immersed in NaCl solution for different durations: (a) EIS results after 1 day of immersion, (b) EIS results after 3 days of immersion, (c) EIS results after 7 days of immersion, (d) Bode results after 1 day of immersion, (e) Bode results after 3 days of immersion, and (f) Bode results after 7 days of immersion.

6 — Angi Chen et al. DE GRUYTER

Table 1: EIS data of coatings with different modifier additions

Time (days)	Samples	Rs (Ω·cm²)	<i>C</i> (Ω ⁻¹ ·cm ⁻² sn)	Rp (Ω·cm²)
1	C _{1.2} P _{0.1} EP C _{1.2} P _{0.15} EP C _{1.2} P _{0.2} EP	9,634 11,844 9,154	1.76 × 10 ⁻⁷ 3.50 × 10 ⁻⁷ 5.44 × 10 ⁻⁶	29,150 45,197 95,593
3	$C_{1.2}P_{0.3}EP$ $C_{1.2}P_{0.1}EP$ $C_{1.2}P_{0.15}EP$	10,104 14,833 14,826	1.15×10^{-5} 1.20×10^{-6} 2.14×10^{-5}	36,970 10,477 11,822
7	$C_{1.2}P_{0.2}EP$ $C_{1.2}P_{0.3}EP$ $C_{1.2}P_{0.1}EP$	15,188 14,282 1,638	1.26×10^{-5} 3.53×10^{-6} 1.29×10^{-4}	14,478 11,136 1,067
	$C_{1.2}P_{0.15}EP$ $C_{1.2}P_{0.2}EP$ $C_{1.2}P_{0.3}EP$	1,635 2,394 1,523	8.22×10^{-5} 4.07×10^{-7} 3.69×10^{-5}	2,561 6,171 2,151

presents capacitive reactance semi-circular arcs with different sizes. The diameter of the semicircle with 0.2 ml modifier is the largest, which indicates that it has the largest impedance value and the best corrosion resistance, and the impedance value is 95,593 $\Omega \cdot \text{cm}^2$ on the first day. It can be seen from Figure 3(b) that on the third day of soaking, the diameters of semicircles with 0.15 and 0.3 ml of modifier are basically the same, and the simulated impedance values are 11,822 and 11,136 Ω·cm², respectively. It can be seen from Figure 4b that on the third day of soaking, the diameters of semicircles with 0.15 and 0.3 ml of modifier are the same, and the simulated impedance values are 11,822 and 11,136 Ω ·cm², respectively. The diameter of the semicircle with 0.2 ml modifier is still the largest, and the impedance value is 14,478 Ω·cm², as can be seen from Figure 3(c), on the 7th day of immersion, the impedance values of the four coatings all decreased to different degrees. The impedance value of $C_1 \circ P_0 \circ EP$ coating (6.171 $\Omega \cdot cm^2$) is about 6 times that of $C_{12}P_{01}EP$ coating (1,067 Ω ·cm²), $C_{12}P_{015}EP$ coating (2,561 Ω ·cm²), and C_{1.2}P_{0.3}EP coating (2,151 Ω ·cm²). The above results show that the corrosion resistance first increases and then decreases with the increase of modifier content. This is because the content of epoxy resin on the surface of the coating decreases when the modifier is added more than 0.2 ml, which

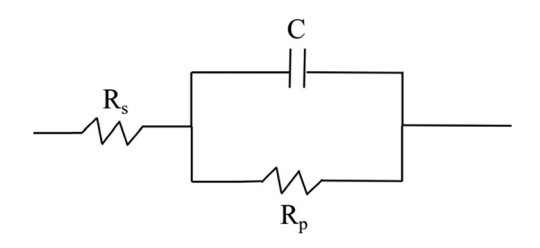


Figure 4: Equivalent electric circuits of the collected EIS results.

reduces the ability to prevent the diffusion of corrosive media in the coating and shortens the path of water and chloride ions entering the substrate. Therefore, it can be proved that the optimum addition amount is 0.2 ml, and the corrosion resistance of the coating is the best.

The better the anticorrosion performance of the organic anticorrosive coating, the higher the Bode modulus, the fewer micropores in the coating, and the greater the pore resistance [27]. The results of the first day of immersion are shown in Figure 3(d), and the modulus value of the coating increases first and then decreases in the low-frequency region. The Bode modulus of 0.2 ml modifier is the largest. close to 10⁵ Ω·cm², indicating that the protective performance of C_{1.2}P_{0.2}EP coating is the best at the initial soaking stage. The results of the third day of immersion are shown in Figure 3(e), and the Bode modulus values of C_{1.2}P_{0.1}EP and C_{1.2}P_{0.3}EP coatings are similar. Among the four coatings, the modulus is the smallest, indicating that the porosity of the coating is the same as that of 0.1 ml when the modifier is added in 0.3 ml, and the modulus is close to $10^4 \ \Omega \cdot \text{cm}^2$. Among the four coatings, the modulus of C_{1.2}P_{0.2}EP coating remains the largest. As shown in Figure 3(f), the results of the seventh day of immersion show that the modulus of C_{1.2}P_{0.2}EP coating differs from that of other coatings, and the modulus remains the largest. According to the Bode modulus value in the low-frequency region in Figure 3(f), it can be directly explained that the corrosion resistance of epoxy resin coating is the best when the modifier addition is 0.2 ml. According to the curve variation in Figure 3(f), it can be concluded that the protective performance of the coatings of each sample group is $C_{1.2}P_{0.2}EP > C_{1.2}P_{0.15}EP > C_{1.2}P_{0.3}EP >$ $C_{1.2}P_{0.1}EP$.

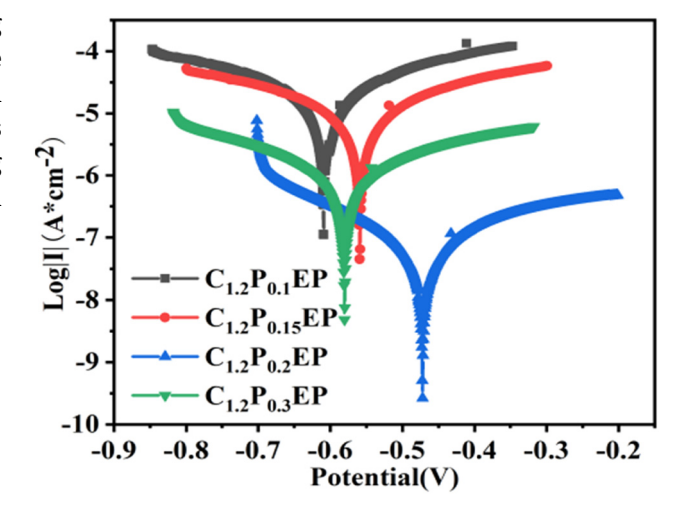


Figure 5: Tafel plots of coatings with various modifiers and addition amounts after immersion in NaCl solution for 7 days.

Four groups of samples with 0.1-0.3 ml modifier were soaked in NaCl solution for seven days, and the electrochemical tests were carried out on each group of samples. The Tafel polarization curves of each group of samples are shown in Figure 5. Generally speaking, a lower E_{coor} or a higher I_{coor} has better corrosion resistance [20]. As seen from Figure 5, with the increase of modifier content, E_{coor} tends to decrease first and then increase. On the contrary, $I_{\rm coor}$ tends to increase first and then decrease. As seen from Figure 6, compared with the other three groups of coatings, the cathodic polarization curve and anodic polarization curve of C_{1.2}P_{0.2}EP coating shifted to the lower right corner, with the highest I_{coor} . Among them, I_{coor} is one order of magnitude higher than other coatings. This indicates that the cathodic and anodic polarization of C_{1.2}P_{0.2}EP coating has the most potent inhibition and the best corrosion resistance.

3.2.2 Effect of Kaolin addition on corrosion resistance of epoxy hydrophobic coatings

The influence of kaolin content on the corrosion resistance of epoxy resin coating was investigated by the control variable method. Figure 6 shows the EIS and Bode of coatings with different kaolin additions immersed in 3.5 wt% NaCl

solution for various durations, and the specific data are presented in Table 2. The larger the bending radius of the impedance arc, the more difficult the corrosion reaction is. As shown in Figure 6(a), on the first day of soaking, the EIS diagram presents semi-circular arcs with different sizes, and the diameter of the semi-circular arc with kaolin addition of 1 g is the largest. This shows it has the largest impedance value and the best corrosion resistance, 47,373 $\Omega \cdot \text{cm}^2$ on the first day. It can be seen from Figure 6(b) that

Table 2: EIS data of coatings with different kaolin additions

Time (days)	Samples	Rs (Ω·cm²)	C (Ω ⁻¹ ·cm ⁻² sn)	Rp (Ω·cm²)
1	$C_{0.5}P_{0.2}EP$	10,406	1.82×10^{-5}	19,354
	$C_1P_{0.2}EP$	9,634	1.94×10^{-5}	47,373
	$C_{1.2}P_{0.2}EP$	9,728	8.36×10^{-6}	29,600
	$C_{1.5}P_{0.2}EP$	9,782	1.10×10^{-6}	28,758
3	$C_{0.5}P_{0.2}EP$	10,418	3.26×10^{-5}	2,943
	$C_1P_{0.2}EP$	10,340	7.62×10^{-5}	20,334
	$C_{1.2}P_{0.2}EP$	10,056	1.54×10^{-4}	6,652
	$C_{1.5}P_{0.2}EP$	10,550	3.54×10^{-5}	3,962
7	$C_{0.5}P_{0.2}EP$	189	1.84×10^{-4}	811
	$C_1P_{0.2}EP$	204	1.19×10^{-4}	1,982
	$C_{1.2}P_{0.2}EP$	161	2.14×10^{-4}	1,598
	$C_{1.5}P_{0.2}EP$	166	2.76×10^{-4}	1,474

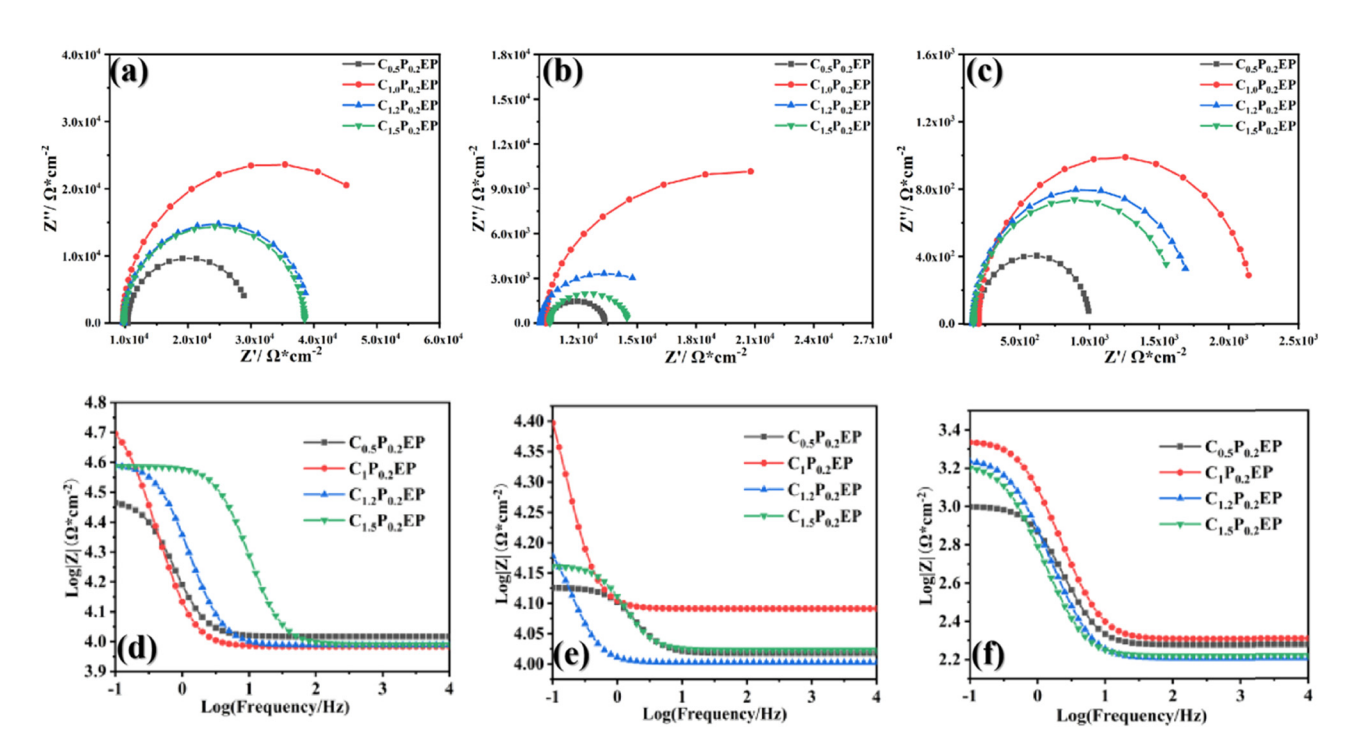


Figure 6: EIS and Bode plots of coatings with different kaolin additions immersed in NaCl solution for different durations: (a) EIS results after 1 day of immersion, (b) EIS results after 3 days of immersion, (c) EIS results after 7 days of immersion, (d) Bode results after 1 day of immersion, (e) Bode results after 3 days of immersion, and (f) Bode results after 7 days of immersion.

on the third day of soaking, the semicircle diameters with kaolin addition of 0.5 and 1.5 g are basically the same, and the simulated impedance values are 2,943 and 3,962 $\Omega \cdot \text{cm}^2$, respectively. The diameter of the semicircle with 1 g modifier remains the largest, and the impedance value is 20,334 $\Omega \cdot \text{cm}^2$. The impedance value of $C_1P_{0.2}EP$ coating is about three times that of C_{1.2}P_{0.2}EP coating and eight times that of $C_{0.5}P_{0.2}EP$ coating and $C_{1.5}P_{0.2}EP$ coating, as can be seen from Figure 6(c), on the 7th day of immersion, the impedance values of the four coatings all decreased to different degrees. The impedance value of C₁P_{0.2}EP coating (1,982 $\Omega \cdot \text{cm}^2$) remains the largest, which is about twice that of $C_{0.5}P_{0.2}EP$ coating (811 $\Omega \cdot cm^2$). The impedance values of $C_{1.2}P_{0.2}EP$ coating (1,598 $\Omega \cdot cm^2$) and $C_{1.5}P_{0.2}EP$ coating (1,474 $\Omega \cdot \text{cm}^2$) are basically the same. The above results show that with the increase of kaolin content, the corrosion resistance first increases and then decreases, which is caused by cracks and protruding points on the coating surface when kaolin content is greater than 1 g. Therefore, it can be proved that the optimum amount of kaolin is 1g, and the corrosion resistance of the coating is the best.

To further analyze the influence of kaolin content on the corrosion resistance of epoxy resin coating, the electrochemical behavior of the coating was deeply analyzed. Figure 6(d)–(f) shows the Bode diagram of four kinds of coatings with different kaolin content immersed in 3.5 wt% sodium chloride solution at different times. The reference index of corrosion resistance of the coating is the low-frequency impedance modulus, and the larger the modulus, the better the corrosion resistance. The results of the first day of immersion are shown in Figure 6(d), and the modulus value of the coating increases first and then decreases in the low-frequency region. The Bode modulus with adding 1 g kaolin is the largest, close to $10^{4.7} \Omega \cdot \text{cm}^2$, indicating that the protective performance of C₁P_{0.2}EP coating is the best at the initial immersion stage. The Bode modulus values of C_{1.2}P_{0.2}EP and C_{1.5}P_{0.2}EP coatings are similar, which shows that the porosity of the coating is the same as that of 1.5 g when the kaolin content is 1.2 g, and the modulus value is close to 10^{4.16} Ω·cm². The results of the third day of immersion are shown in Figure 6(e), and the modulus of C_{0.5}P_{0.2}EP coating is the smallest among the four coatings. There is an obvious gap between the modulus values of C₁P_{0.2}EP coating and other coatings, and the modulus value remains the largest. The results of the seventh day of immersion are shown in Figure 6(f), and the modulus of C₁P_{0.2}EP coating remains the largest among the four coatings. According to the Bode modulus in the low-frequency region in Figure 6, it can be directly explained that the corrosion resistance of EP coating is the best when the kaolin content is 1 g. According to the curve variation in Figure 6, it can be concluded that the

protective performance of the coatings of each sample group is $C_1P_{0.2}EP > C_{1.2}P_{0.2}EP > C_{1.5}P_{0.2}EP > C_{0.5}P_{0.2}EP$.

The Tafel polarization curves of four kinds of kaolin coatings with different contents are shown in Figure 7. As shown in Figure 7, the cathodic polarization curve and anodic polarization curve of $C_1P_{0.2}EP$ coating shifted to the lower right corner compared with the other three groups of coatings, which indicated that the cathodic polarization and anodic polarization of $C_1P_{0.2}EP$ coating were the strongest. A comparison of $C_{0.5}P_{0.2}EP$, $C_1P_{0.2}EP$, $C_{1.2}P_{0.2}EP$, and $C_{1.5}P_{0.2}EP$ coatings shows that when corrosion occurs, $C_1P_{0.2}EP$ coating is more effective than the other three coatings in prolonging the path of corrosion penetration and delaying the time of corrosion occurrence. The above results show that the barrier performance of kaolin to corrosive electrolytes such as water and chloride ions is the best when the amount of kaolin is 1 g.

3.3 Salt spray resistance test

The long-term corrosion resistance of different kaolin additions' coatings in a robust corrosive environment was studied by a neutral salt spray test with 3.5 wt% sodium chloride. Figure 8 is a photo of the samples of the neutral salt spray test for 300 h. The pieces a–e are EP, $C_{0.5}P_{0.2}EP$, $C_{1.2}P_{0.2}EP$, $C_{1.0}P_{0.2}EP$, and $C_{1.5}P_{0.2}EP$, respectively.

According to Figure 8(a), after 200 h of salt spray, tiny bubbles appeared on the steel substrate surface protected by EP coating in the blank group. There were many red rust corrosive products, and the corrosion area was

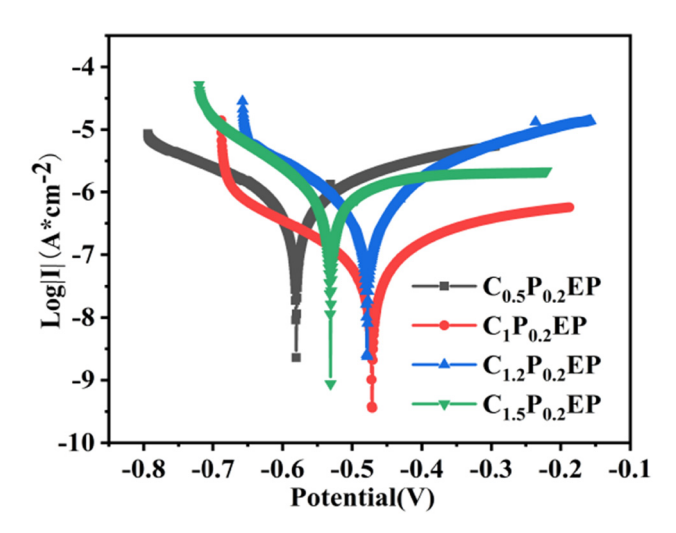


Figure 7: Tafel curves of coatings with different kaolin additions immersed in 3.5 wt% sodium chloride solution for 7 days.

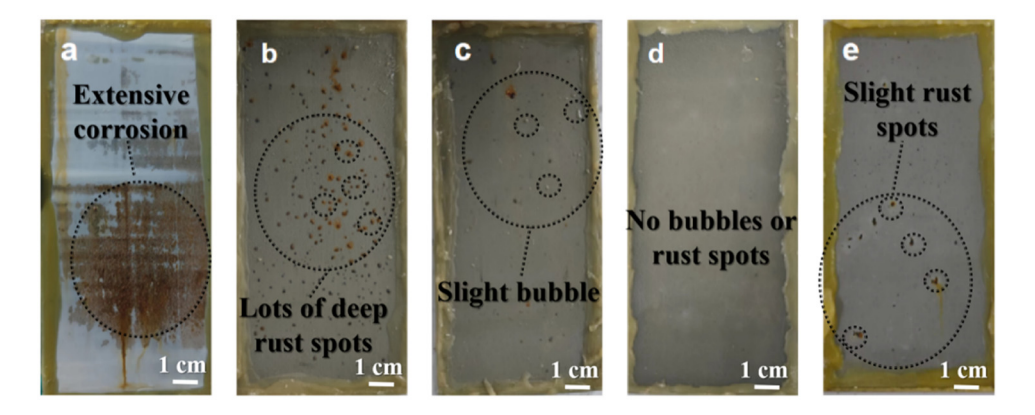


Figure 8: (a) Content of C0P0.2EP, (b) content of C0.5P0.2EP, (c) content of C1.2P0.2EPd, (d) content of C1.0P0.2EP, (e) content of C1.5P0.2EP.

relatively large and tended to spread outward. Figure 8(b) shows the results of the C_{0.5}P_{0.2}EP coating after 300 h in a salt spray chamber. It can be seen from the figure that there are numerous rust spots on the coating, and the color of the rust spots is relatively dark. However, there are no signs of extensive corrosion, indicating that the addition of kaolin effectively slows down the corrosion rate. Figure 8(c) displays the results of the C_{1,2}P_{0,2}EP coating after 300 h in a salt spray chamber. The figure reveals that there are slight bubbles on the coating but no extensive rust spots, indicating a significant improvement in corrosion resistance compared to the C_{0.5}P_{0.2}EP coating. Figure 8(d) demonstrates the results of the C_{1.0}P_{0.2}EP coating after 300 h in a salt spray chamber. It is evident from the figure that there are no bubbles or rust spots on the coating, and it remains unchanged. Therefore, the corrosion resistance of the C_{1.0}P_{0.2}EP coating is further enhanced compared to the C_{1.2}P_{0.2}EP coating. Figure 8(e) illustrates the results of the C_{1.5}P_{0.2}EP coating after 300 h in a salt spray chamber. Although there are no bubbles on

the coating, a few rust spots are present, indicating a decrease in corrosion resistance compared to the C_{1.0}P_{0.2}EP and C_{1.2}P_{0.2}EP coatings. Overall, the C_{1.0}P_{0.2}EP coating exhibits the best corrosion resistance. It shows that adding kaolin nanosheets effectively enhances the barrier properties of the epoxy resin coating surface and the bonding strength between the coating and the steel substrate. This shows that C₁P_{0.2}EP coating may further inhibit the electrolyte solution from penetrating the substrate surface and has excellent corrosion resistance.

3.4 Wear resistance test and self-cleaning experiment

For the C_{1.0}P_{0.2}EP coating, we conducted a wear resistance test as shown in Figure 9. Figure 9(a) shows the wear test setup, while Figure 9(b) illustrates the change in the hydrophobic angle during the wear test. As can be seen from

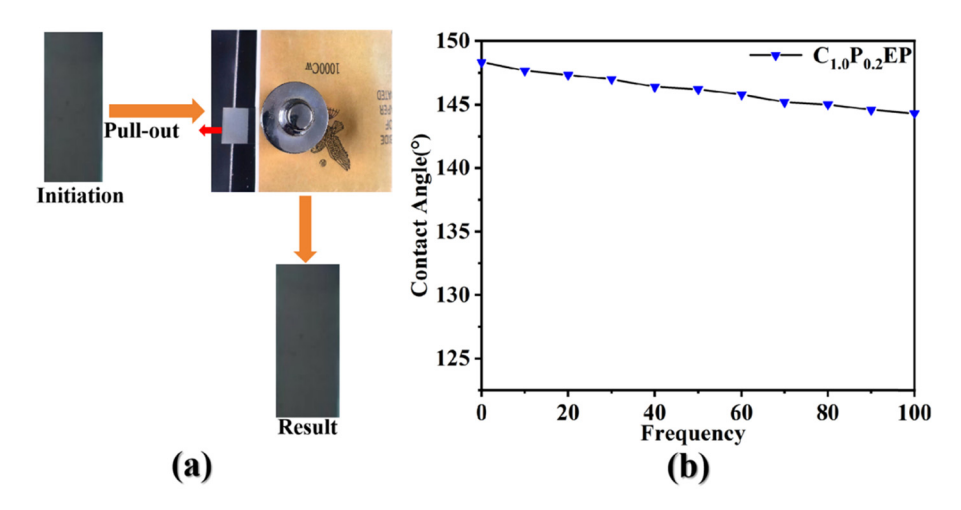
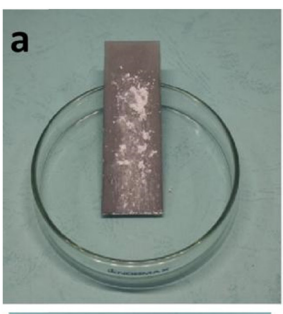


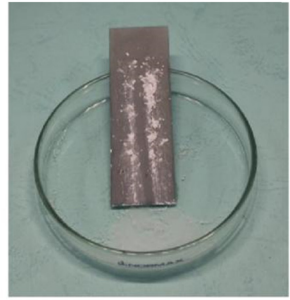
Figure 9: Wear resistance diagram: (a) wear resistance experiment process and (b) contact angle change curve.

Figure 9(a), after 100 wear cycles, the coating surface exhibited no cracking, powder shedding, or significant wear marks, demonstrating its excellent wear resistance. In Figure 9(b), it is evident that the hydrophobic angle of the coating gradually decreased with increasing friction cycles, but the trend was relatively gradual. After 100 friction cycles, the contact angle decreased by only 4° , indicating that the coating still maintained excellent hydrophobicity and reflected its superior wear resistance. Overall, the $C_{1.0}P_{0.2}EP$ coating exhibits outstanding mechanical wear resistance.

In addition, self-cleaning performance is one of the specific properties of hydrophobic materials. To test the self-cleaning and anti-fouling ability of the prepared composite materials, two testing methods were adopted. One is to scatter powdery pollutants on the material's surface, drop water droplets from above the sample, and observe the self-cleaning effect of the composite material. The other is to soak the prepared material in sewage for some time and then take it out to observe whether there is any dirt residue on the surface of the material. In the test, hydrophilic alumina powder and sediment act as pollutants, and Figure 10 shows the test process of self-cleaning. As shown in Figure 10(a), hydrophilic alumina powder will roll off with the water drops dripping on the material's surface, thus completing the effect of cleaning the surface. This phenomenon occurs because pollutant particles are readily adsorbed on water droplets, and the adhesion of water droplets to composite materials is weak. As shown in Figure 10(b), the prepared







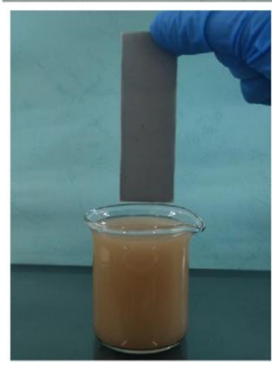


Figure 10: Self-cleaning ability test of (a and b) $C_{1.2}P_{0.1}EP$ coating.

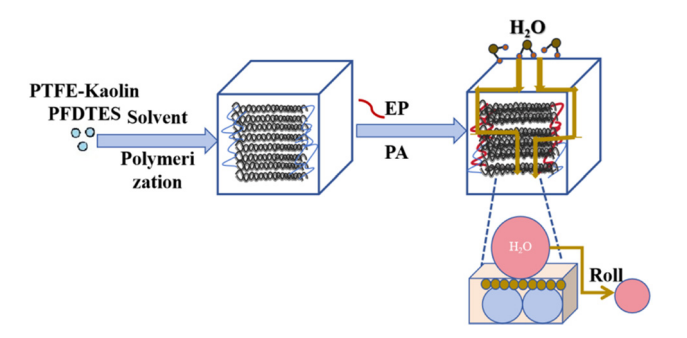


Figure 11: Diagram of anticorrosion mechanism.

material is immersed in muddy water and taken out after 30 s. After observing the surface of the composite material, there is little difference from that before immersion, and there is no sign of being polluted by muddy water, which further confirms the superior self-cleaning property of the prepared material. In addition to the above tests on the materials made on the glass substrate, the same tests were carried out on the materials coated on the substrates, such as wood, ceramics, and copper sheets. The results of the above tests show that the material has self-cleaning performance, which can effectively prevent the pollution of pollutants in practical application, and the substrate does not limit the coating.

3.5 Corrosion resistance mechanism

The anticorrosion mechanism of the C_{1.0}P_{0.2}EP coating is illustrated in Figure 11. Under the action of modifiers, kaolin and PTFE polymerize in an anhydrous ethanol solvent to form a three-dimensional stacked structure. This structure, combined with EP and PA as binders, creates a thin film with excellent hydrophobic properties. When water and oxygen molecules in the air contact the film, the oxygen molecules penetrate the pores and reach the substrate. However, the water molecules roll along the hydrophobic film, increasing the path they need to take to enter the film. This extended path lengthens the time it takes for water molecules to reach the substrate, thereby delaying the occurrence of corrosion reactions on the substrate and enhancing the coating's anticorrosion capabilities. Therefore, the $C_{1.0}P_{0.2}EP$ coating exhibits excellent corrosion resistance.

4 Conclusions

This study fabricated a hydrophobic thin film through a simple mixing method, utilizing kaolin and PTFE as

additive particles, PFDTES as a modifier, and EP and PA as adhesives and determined the optimal performance of the C₁P_{0.2}EP coating by controlling variables. After soaking the coating in a 3.5 wt% NaCl solution for 1, 3, and 7 days, it exhibited maximum impedance radii of 47,373, 20,334, and 1,982 Ω·cm², respectively. Additionally, it demonstrated the highest Bode modulus values, as well as the largest $E_{\rm corr}$ and the smallest I_{corr} , proving its superior corrosion resistance. After 300 h in a salt spray chamber with a 3.5 wt% NaCl solution, the C₁P_{0.2}EP coating showed no rust spots or bubbles compared to other coatings, further emphasizing its excellent corrosion resistance. Furthermore, the wear resistance and self-cleaning capabilities of the C₁P_{0.2}EP coating were also tested. The results indicated that, under the action of a 500 g weight and 1,000 mesh sandpaper, the coating exhibited no cracking or powder shedding after 100 abrasion cycles. Additionally, there were no visible scratches on the surface. Notably, the contact angle of the coating only decreased by 4° after 100 cycles, demonstrating its excellent mechanical wear resistance. Dry powder and solution self-contamination experiments were conducted on the coating. The results showed that neither soil particles applied to the coating's surface nor immersion in dirty water caused any adhesion. The coating maintained its self-cleaning ability, thus exhibiting excellent self-cleaning capabilities.

Overall, the $C_1P_{0.2}$ EP hydrophobic coating not only possesses excellent corrosion resistance but also demonstrates superior wear resistance and self-cleaning abilities. Therefore, it holds promising application prospects in anticorrosion coatings.

Acknowledgments: The authors acknowledge that this work has been supported by the National Natural Science Foundation of China under Grant No. 52102119, Young Elite Scientists Sponsorship Program by CAST (No. 2022QNRC001).

Funding information: This study was financially supported by the Fujian Provincial Department of Education Youth Project (Project No. JAT200650); Nanping Resource Chemical Industry Science and Technology Innovation joint funding project (No. N2021Z003); Wuyi University Service Industry Research Project (No. 2021XJFWCY03); Wuyi University Talent Introduction research start-up fund project (No. YJ202309); and Innovation and Entrepreneurship Training Program for College Students (No. S202210397076, 202310397026).

Author contributions: Anqi Chen: writing – original draft, Yan Zhao: investigation, Hongda Chen: formal analysis, Anqi Chen and HuaChao Ma: visualization, project administration; Kuilin Lv and Yan Zhao: writing – review and

editing, funding acquisition. All authors have accepted responsibility for the entire content of this manuscript and approved its submission.

Conflict of interest: The authors state no conflict of interest.

References

- [1] Wu, C., J. Wang, S. Song, Z. Wang, and S. Zhao. Antifouling and anticorrosion performance of the composite coating made of tetrabromobisphenol-A epoxy and polyaniline nanowires. *Progress in Organic Coatings*, Vol. 148, 2020, id. 105888.
- [2] Yuan, C. D., M. Zhao, D. Sun, L. Yang, L. Zhang, R. W. Guo, et al. Preparation and properties of few-layer graphene modified waterborne epoxy coatings. *Journal of Applied Polymer Science*, Vol. 135, No. 41, 2018, id. 46743.
- [3] Ye, Y., D. W. Zhang, T. Liu, Z. Liu, J. Pu, W. Liu, et al. Superior corrosion resistance and self-healable epoxy coating pigmented with silanzied trianiline-intercalated graphene. *Carbon*, Vol. 142, 2019, pp. 164–176.
- [4] Ye, Y., D. W. Zhang, T. Liu, Z. Liu, W. Liu, J. Pu, et al. Improvement of anticorrosion ability of epoxy matrix in simulate marine environment by filled with superhydrophobic POSS-GO nanosheets. *Journal of Hazardous Materials*, Vol. 364, 2018, pp. 244–255.
- [5] Tan, X., Y. M. Wang, Y. T. Tu, T. Xiao, S. Alzuabi, Y. P. Xiang, et al. Icephobicity studies of superhydrophobic coating on aluminium. *Surface Engineering*, Vol. 37, No. 10, 2021, pp. 1239–1245.
- [6] Schlaich, C., M. Li, C. Cheng, L. Donskyi, L. Yu, G. Song, et al. Mussel-inspired polymer-based universal spray coating for surface modification: Fast fabrication of antibacterial and superhydrophobic surface coatings. *Advanced Materials Interfaces*, Vol. 5, 2018, id. 1701254.
- [7] Nakajima, A., K. Hashimoto, and T. Watanabe. Recent studies on super-hydrophobic films. *Monatshefte Fur Chemie Chemical Monthly*, Vol. 132, 2001, pp. 31–41.
- [8] Wu, Y., K. Liu, B. Su, and L. Jiang. Superhydrophobicity-mediated electrochemical reaction along the solid-liquid-gas triphase interface: Edge-growth of gold architectures. *Advanced Materials*, Vol. 26, 2014, pp. 1124–1128.
- [9] Cui, Y., L. Zhang, C. Xing, and Y. Tan, et al. Anti-icing properties and application of superhydrophobic coatings on asphalt pavement. *Construction and Building Materials*, Vol. 419, 2024, id. 135452.
- [10] Liu, S., L. Gu, H. Wang, H. Zhao, J. Chen, H. Yu, et al. Corrosion resistance of grapheme-reinforced waterborne epoxy coatings. *Journal of Materials Science & Technology*, Vol. 32, 2015, pp. 1223–1230.
- [11] Fu, Y., F. Xu, D. Weng, X. Li, Y. Li, J. Sun, et al. Superhydrophobic foams with chemical and mechanical damage healing abilities enabled by self-healing polymers. ACS Applied Materials & Interfaces, Vol. 11, 2019, pp. 37285–37294.
- [12] González-García, Y., S. González, and R. M. Souto. Electrochemical and structural properties of a polyurethane coating on steel substrates for corrosion protection. *Corrosion Science*, Vol. 49, No. 9, 2007, pp. 3514–3526.

- [13] Yang, Z., L. Wang, W. Sun, S. Li, T. Zhu, W. Liu, et al. Superhydrophobic epoxy coating modified by fluorographene used for anti-corrosion and self-cleaning. *Applied Surface Science*, Vol. 401, 2017, pp. 146–155.
- [14] Syed, J. A., S. Tang, H. Lu, and X. Meng. Smart PDDA/PAA multilayer coatings with enhanced stimuli responsive self-healing and anticorrosion ability. *Colloids and Surfaces A: Physicochemical and Engineering Aspects*, Vol. 476, 2015, pp. 48–56.
- [15] Rasitha, T. P., N. G. Krishna, B. Anandkumar, S. Vanithakumari, and J. Philip. A comprehensive review on anticorrosive/antifouling superhydrophobic coatings: Fabrication, assessment, applications, challenges and future perspectives. Advances in Colloid and Interface Science, Vol. 324, 2024, id. 103090.
- [16] Jena, G., C. Thinaharan, R. P. George, and J. Philip. Robust nickelreduced graphene oxide-myristic acid superhydrophobic coating on carbon steel using electrochemical codeposition and its corrosion resistance. Surface and Coatings Technology, Vol. 397, 2020, id. 125942.
- [17] Zhu, X., Z. Zhang, and X. Men. Robust superhydrophobic surfaces with mechanical durability and easy repairability. *Journal of Materials Chemistry*, Vol. 21, 2011, pp. 15793–15797.
- [18] Cao, C., B. Yi, J. Zhang, C. Hou, Z. Wang, G. Lu, et al. Sprayable superhydrophobic coating with high processibility and rapid damage-healing nature. *Chemical Engineering Journal*, Vol. 392, 2020, id. 124834.
- [19] Jena, G. and J. Philip. A review on recent advances in graphene oxide-based composite coatings for anticorrosion applications. *Progress in Organic Coatings*, Vol. 173, 2022, id. 107208.

- [20] Chang, K., M. Hsu, H. Lu, M. Lai, P. Liu, C. Hsu, et al. Room-temperature cured hydrophobic epoxy/graphene composites as corrosion inhibitor for cold-rolled steel. *Carbon*, Vol. 66, 2014, pp. 144–153.
- [21] Liu, S., L. Gu, H. Zhao, J. Chen, and H. Yu. Corrosion resistance of grapheme-reinforced waterborne epoxy coatings. *Journal of Materials Science & Technology*, Vol. 32, 2015, pp. 1223–1230.
- [22] Lv, K., D. Wan, R. Pan, W. Suo, and Y. Zhu. Curvature of NCNTs induced selectivity of CO₂ electroreduction into CO. *Carbon Neutralzation*, Vol. 1, 2022, pp. 189–197.
- [23] Zhang, D., L. Zhuo, and Q. Xiang. Electrophoretic deposition of polytetrafluoroethylene (PTFE) as anti-corrosion coatings. *Materials Letters*, Vol. 346, 2023, id. 134524.
- [24] Wang, X., F. Tang, X. Qi, and Z. Lin. Mechanical, electrochemical, and durability behavior of graphene nano-platelet loaded epoxyresin composite coatings. *Composites Part B: Engineering*, Vol. 176, 2019, id. 107103.
- [25] Wang, X., B. B. Wang, W. Yang, Q. Zhao, Z. M. Xu, and W. M. Yan. Fabrication of stable and versatile superhydrophobic PTFE coating by simple electrodeposition on metal surface. *Progress in Organic Coatings*, Vol. 172, 2022, id. 107090.
- [26] Tang, F., G. Chen, J. S. Volz, R. K. Brow, and M. Koenigstein. Microstructure and corrosion resistance of enamel coatings applied to smooth reinforcing steel. *Construction and Building Materials*, Vol. 35, 2012, pp. 376–384.
- [27] Selvaraj, M. and M. Natesan. Influence of dicyclohexylamlne nitrite in epoxy primer. *Bulletin of Electrochemistry*, Vol. 15, No. 2, 1999, pp. 87–90.